



# Rubidium-modified bioactive glass-ceramics with hydroxyapatite crystals for bone regeneration

Yan-ni TAN, Wen-juan CHEN, Wei WEI, Qian-li HUANG, Xiang HE

State Key Laboratory of Powder Metallurgy, Central South University, Changsha 410083, China

Received 20 March 2020; accepted 25 November 2020

**Abstract:** In order to study the influence of rubidium (Rb) addition on the phase composition, microstructure, mechanical properties and cell response of bioactive glass-ceramics,  $\text{CaO-SiO}_2\text{-Na}_2\text{O-B}_2\text{O}_3\text{-MgO-ZnO-P}_2\text{O}_5$  glass system was designed with and without addition of Rb. The results show that hydroxyapatite (HA) and Mg-whitelockite ( $\text{Ca}_{18}\text{Mg}_2\text{H}_2(\text{PO}_4)_{14}$ ) crystalline phases are formed in the glass matrix without Rb. After the addition of Rb, only HA phase is detected. The grain size of the crystals in the glass-ceramics is larger with the addition of Rb than that of samples without Rb. Rb addition can improve the bending strength of glass-ceramics. The cultivation of human bone marrow mesenchymal stem cells (hBMSCs) on Rb-containing glass-ceramics demonstrates enhanced cell adhesion, proliferation and ALP activity. In conclusion, Rb-modified glass-ceramics exhibit good mechanical property, excellent bioactivity and biocompatibility, which have potential for bone regeneration application.

**Key words:**  $\text{CaO-SiO}_2\text{-Na}_2\text{O-B}_2\text{O}_3\text{-MgO-ZnO-P}_2\text{O}_5$ ; rubidium; bioactive glass-ceramics; hydroxyapatite; human bone mesenchymal stem cells

## 1 Introduction

Orthopedic and dental clinicians often encounter bone defects during operations for fractures, bone infections, tumors, and so on. Artificial materials implanted into bone defects are generally encapsulated by fibrous tissue and isolated from the surrounding bone tissue. This is the normal response of the body towards inert artificial materials [1]. In 1971, HENCH and his coworkers [2] firstly reported the bone bonding properties of bioactive glasses. Since then, various types of ceramic, glass and glass-ceramic materials have been proposed and used to repair or replace the damaged bone in many clinical applications.

Glass-ceramics contain nano- and/or micro-grained polycrystalline phases embedded in residual glass phase, which are prepared by the well-controlled heat treatment following the progressions

of nucleation and crystal growth within the glass matrix [3]. Due to the controlled devitrification and evolution of variable proportions of crystalline and glassy phases, glass-ceramics substantially overcome the shortcomings encountered in glasses. These are acknowledged with the special status of functional biomaterials that have superior performance with tailorable manufacturing and convenient designs [4]. Bioactive glass-ceramics are those types of glass-ceramics that have the ability to form chemical bond with bone through the formation of a biologically active apatite layer after reaction with the surrounding body fluid [5]. The general characteristics of these types of glass-ceramics are that they contain CaO and  $\text{P}_2\text{O}_5$  in their chemical composition, and they contain apatite  $\text{Ca}_{10}(\text{PO}_4)_6(\text{F},\text{Cl},\text{OH})_2$  as one of the crystal phases [3], such as Cerabone A-W, Bioverit and Ceravital [4]. Hydroxyapatite ( $\text{Ca}_{10}(\text{PO}_4)_6(\text{OH})_2$ , HA) has excellent bioactivity and biocompatibility

as it is similar with the inorganic chemical composition of the tooth and bone of vertebrate [6]. Thus, it has been widely studied and used in biomedical field.

Since the pioneering invention of 45S5 Bioglass, several other glass and glass-ceramic compositions have been developed to improve the properties and clinical abilities of traditional bioactive glass to meet the stringent requirements of repairing and regeneration of damaged bones [4]. One trend is the incorporation of different elements into the composition of these bioactive glasses and glass-ceramics to enhance their physical characteristics and therapeutic benefit [5], such as silver (Ag), magnesium (Mg), strontium (Sr), zinc (Zn), silicon (Si), fluoride (F), potassium (P) and zirconia ( $ZrO_2$ ) [7,8]. For example, the addition of BaO and  $TiO_2$  can effectively improve the bioactivity of the host glass [9,10]. The addition of  $Ag_2O$  in 45S5 Bioglass could endow the material with bacteriostatic and bactericidal properties [11]. Sr-substituted bioactive glass may promote an anabolic effect on osteoblasts and an anti-catabolic effect on osteoclasts [12]. A further research showed that the incorporation of Sr into mesoporous bioactive glass scaffolds has significantly stimulated the alkaline phosphatase (ALP) activity and osteogenesis/cementogenesis related gene expressions in periodontal ligament cells [13].

Rubidium (Rb) is an alkali metal element along with Li, Na, K and Cs, and has similar biological functions with K. Along with the progress of Rb mining and extraction technology, Rb has attracted more and more attentions and gained wide applications in energy, nonlinear optical crystals, catalysis, medicine, solder, special glass and ferromagnetic materials etc [14]. Rb is also an essential trace element or micronutrient in human body and has very low toxicity. It is excreted mainly through urine [15]. Rb ions have been used

to treat several psychiatric and non-psychiatric conditions including mania, epilepsy, and depression during the last century [16]. However, the addition of Rb in a biomaterial and its effect on the mechanical behavior and biological properties of the biomaterial is rarely studied to our knowledge. In our previous study, it was found that Rb-doped biomaterials have significant effect on promoting the middle and late stage of osteoblastic differentiation [17] as well as improving the angiogenic and osteogenic capacity [18]. Meanwhile, most importantly, it also has good antibacterial properties [17–19]. Rb has been proven to be an effective element for the modification of biomaterials.

The primary aim of this study is to develop bioactive glass-ceramics using the traditional melting method by incorporating varying amounts of Rb and to investigate the effects of rubidium addition in  $CaO-SiO_2-Na_2O-B_2O_3-MgO-ZnO-P_2O_5$  glass-ceramic system on the crystalline phases, mechanical property, bioactivity and cell response of the material.

## 2 Experimental

### 2.1 Preparation of glass-ceramics

The raw materials were reagent grade chemicals without any further purification. The chemical compositions of the glass are displayed in Table 1. The theoretical mole fractions of the addition of Rb salt are 0, 3%, 6% and 10%, respectively. Firstly, the chemicals were fully blended by ball milling for 24 h, and then melted in a corundum crucible at 1300 °C for 2.5 h in an electric furnace. The melted liquid glass was poured into the graphite mold that was preheated at 540 °C for 1 h. Then, the glass samples with the mold were immediately moved into the preheated furnace (550 °C) for the stress relief annealing for 1.5 h, and then cooled with the furnace. Finally, the glass

**Table 1** Chemical compositions of glass-ceramics

Sample No.	Rb content/at. %	Chemical composition/wt. %						
		CaO	$SiO_2$	$B_2O_3$	$Na_2O$	MgO	ZnO	$Ca(H_2PO_4)_2$
1	0	21.2	17.6	16.9	4.9	4.9	4.9	29.6
2	3	20	16.7	16	4.7	4.7	4.7	28.3
3	6	19	15.8	15.2	4.4	4.4	4.4	27
4	10	17.9	14.7	14.1	4.1	4.1	4.1	25.1

samples were heat-treated at 750 °C for 6 h for the nucleation and growth of the crystals. After cooling with furnace, the glass-ceramic samples were obtained.

## 2.2 Characterizations

Differential scanning calorimetry (DSC) was performed with a SDT Q600 thermal analyzer against  $\alpha$ -alumina powder as the reference material. Nonisothermal experiments were performed by heating four kinds of glass powders at a heating rate of 10 °C/min in the range from ambient temperature to 1000 °C.

The crystalline phases formed in the glass-ceramics were identified with X-ray powder diffraction (XRD) equipment (SIMENS D500) with Cu target and Ni filter from  $2\theta=5^\circ$  to  $65^\circ$ . The scanning speed was 2 (°)/min with the step-length of 0.02°, and the accelerated voltage was 40 kV. X-ray photoelectron spectroscopy (XPS, Pekrin-Elmer pHI-5400, USA) and Fourier transform infrared spectroscopy (FTIR, Thermo/USA Nicolet Nexus 670FTIR) were also used to characterize the chemical state and chemical groups.

The scanning electron microscope (SEM, Quanta FEG 250) was used to observe the microstructures of the samples. Before sputtering gold, the glass-ceramics were polished, and chemically-etched using 10% HF solution for 70 s.

## 2.3 Mechanical properties measurement

The bending strength of the glass-ceramics was measured by the three-point bending method with a loading speed of 0.5 mm/min. Six polished rectangular bars with the dimensions of 25 mm × 12 mm × 7 mm were used for each condition.

## 2.4 In vitro bioactivity evaluation

Four groups of glass-ceramic samples were soaked into stimulated body fluid (SBF) for 14 d to test their in vitro bioactivity. The ion concentrations of SBF and the preparation method were the same with those published before [20]. The samples were washed by acetone and distilled water and then dried before soaking. SBF was refreshed every day.

## 2.5 Cell culture

Primary human bone mesenchymal stem cells (hBMSCs) and the appropriate complete medium were purchased from Shanghai Zhongqiaoxinzhou

Biotechnology Co., Ltd. Cells were sub-cultured to the third passage to be used for the biological experiments. All the samples were sterilized by autoclaving sterilizer for 30 min and then dried in the oven at 60 °C.

### 2.5.1 Cell proliferation activity testing

For comparison, samples No. 1 (without Rb) and 4 (10% Rb) were selected for the MTT assay (the methylthiazolyldiphenyl-tetrazolium bromide, Sigma). hBMSCs were cultured on the surface of the samples for 1, 3 and 7 d using 24-well plate. After cultivation for the set time, MTT was added into the well. After 4 h, 1 mL dimethyl sulfoxide (DMSO, VETEC) was added per well. The cell proliferation activity was performed by measuring the OD values at 490 nm using Bio-Tek microplate readers.

### 2.5.2 Cell adhesion and activity assay

After 24 h of cell culture, hBMSCs were rinsed with phosphate buffer and fixed with 2.5% glutaraldehyde, and then sequentially dehydrated by gradient alcohol. After being freeze-dried, the samples were coated with Au for SEM observation.

After culture for 1 and 7 d, the cells on each specimen were washed twice with PBS for 5 min, and then fixed with 4% paraformaldehyde (PFA). After being washed for 3 times by phosphate buffer saline (PBS) for 10 min, the cells were permeabilized with 0.5% TritonX-100 for 5 min at 37 °C. Finally, their cell nuclei and cytoskeleton were stained by 4',6-diamidino-2-phenylindole (DAPI, blue) and FITC-phalloidin (green) in dark, respectively, and observed with a fluorescence microscopy (Motic, China).

### 2.5.3 Alkaline phosphatase activity (ALP) assay

The hBMSCs were cultured on the surfaces of Samples 1 and 4 to compare the effect of Rb addition. At each time point, day 1, day 7 and day 14, the ALP activity of hBMSCs was measured using an ALP kit (Nanjing Jiancheng Bio-engineering Institute, China). It was based on the decomposition effect of benzene disodium phosphate by ALP. Free phenol that was formed after the decomposition can react with 4-aminoantipyrine in alkaline solution and then oxidized by potassium ferricyanide to form red quinone derivatives. The enzyme activity can be measured according to the shades of red. OD values were measured at 520 nm. ALP activity was then calculated according to a standard curve of ALP.

### 2.5.4 Statistical analysis

The data were calculated by mean±standard deviation (SD). Some results were statistically analyzed by one-way analysis of variance (ANOVA) at a significance level of 0.05. If the obtained  $p < 0.05$ , the two groups of data were considered significantly different. If the obtained  $p > 0.05$ , the two groups of data were considered insignificantly different.

## 3 Results and discussion

The DSC curves of the four groups of glass-ceramic powders are shown in Fig. 1. It is obvious that there is only one exothermic peak for all the samples. The addition of Rb does not have significantly influence on the crystallization temperature.

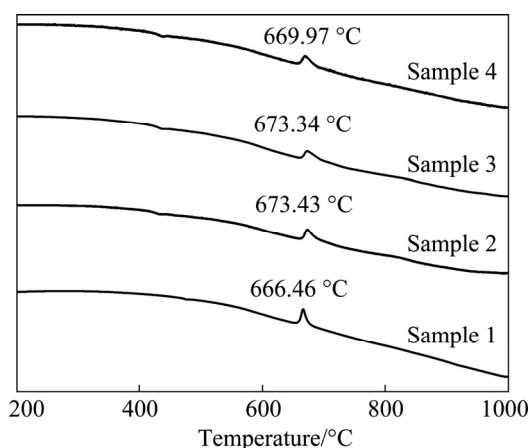


**Fig. 1** DSC curves of four kinds of glass powders with heating rate of 10 °C/min

The XRD patterns of glass-ceramics with different contents of Rb after heat treatment at 720 °C for 6 h are shown in Fig. 2. There are two crystalline phases formed in glass-ceramic without Rb, which are the main phase of hydroxyapatite (HA, PDF #86-0740) and the minor phase of Mg-whitelockite ( $\text{Ca}_{18}\text{Mg}_2\text{H}_2(\text{PO}_4)_{14}$ , PDF#70-2064). The peak intensity of the later one is relatively weak, partly because of the less content of Mg oxides in the start material. After addition of Rb, Mg-whitelockite has not been detected and only HA phase is formed, indicating that Rb addition inhibits the formation of Mg-whitelockite crystals. The content of Rb addition has no significant influence on the HA phase. The diffraction area of the amorphous peak obtained by Rietveld refinement is about 45%–55%.

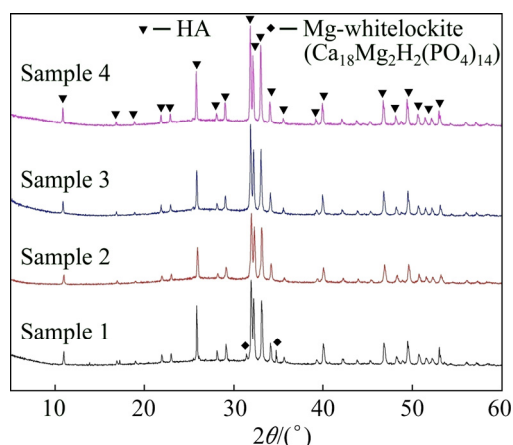


**Fig. 2** XRD patterns of glass-ceramics with different contents of Rb

XPS patterns of glass-ceramics with different contents of Rb are shown in Fig. 3. Sample 1 contains P, Ca and O. For Rb-doped Samples 2–4, additional peaks corresponding to Rb are detected (Fig. 4(a)). The difference of the peaks can be obviously seen between the glass-ceramics with and without Rb (Fig. 4(b)). The peak at 110.4 eV of samples with Rb is the bending energy of Rb (3d). There is no Rb (3d) peak for the sample without Rb. With the increase of the content of Rb, the peak intensity of Rb (3d) increases, proving the successful addition of different contents of Rb ions in the glass-ceramic matrix.

FTIR spectra are shown in Fig. 4. The bands at 578 and 622  $\text{cm}^{-1}$  are attributed to the vibrational modes of P—O bending of HA. The bands observed between 800 and 1200  $\text{cm}^{-1}$  (1035  $\text{cm}^{-1}$ ) can be attributed to the superimposition of P—O antisymmetric stretch in  $\text{PO}_4^{3-}$  of HA phase and Si—O—Si stretching vibrational modes of the glass. The band at 470  $\text{cm}^{-1}$  is resulted from the Si—O—Si bending and the band at 715  $\text{cm}^{-1}$  is associated with large 3D silica structures (Si—O—Si, Si—OH, or SiO—) of the glass [21]. Some bands between 1200 and 1400  $\text{cm}^{-1}$  are the B—O vibrations of  $\text{BO}_3$  units of the glass [22]. The bands observed at 3420  $\text{cm}^{-1}$  of the samples containing Rb belong to the stretching vibrations of O—H. There is no band at 3420  $\text{cm}^{-1}$  of the samples without Rb. The pair of weak peaks at 2002 and 1932  $\text{cm}^{-1}$  can be attributed to  $^{10}\text{B—O}$  and  $^{11}\text{B—O}$  antisymmetric stretching  $\nu_3$  mode of the linear  $\text{BO}_2^-$  groups, respectively [23]. After being compared with references [23,24] and

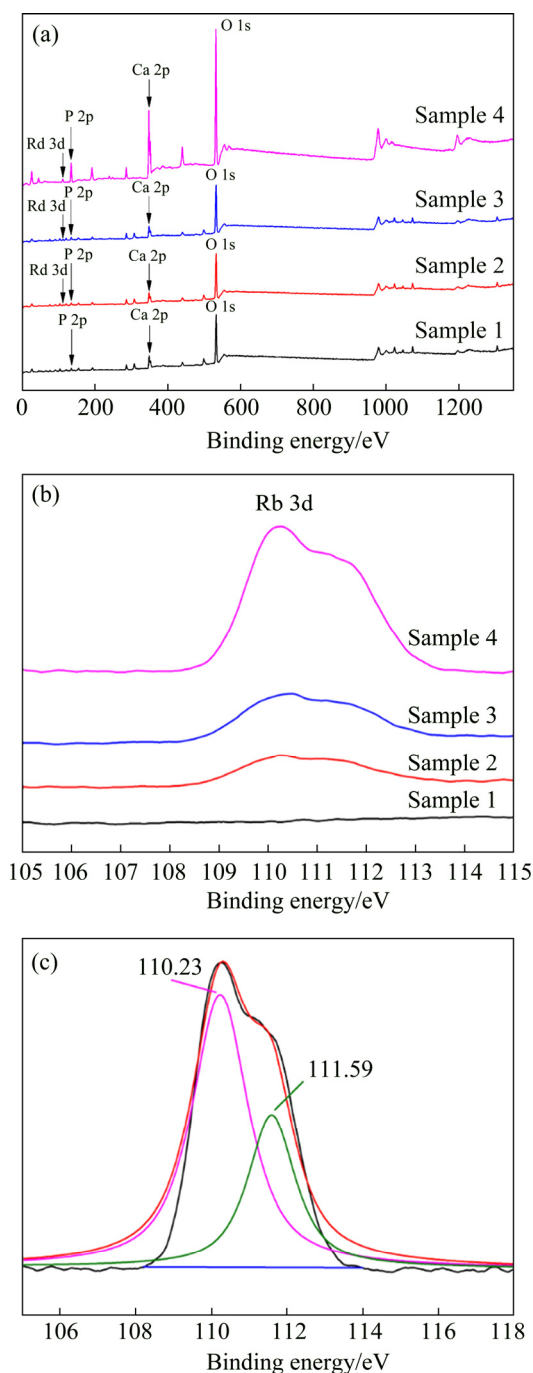


**Fig. 3** XPS patterns of glass-ceramics with different contents of Rb: (a) Full spectra of various specimens; (b) Narrow-spectra of Rb 3d; (c) Rb 3d spectrum of Sample 4

through analysis, it can be inferred that the borate groups belong to HA but not glass. Some phosphate and OH groups of HA were partially substituted by borate groups. In addition, the content of borate substituted HA is maybe under the XRD detection limit or it is amorphous, so there are no related XRD peaks in Fig. 2.

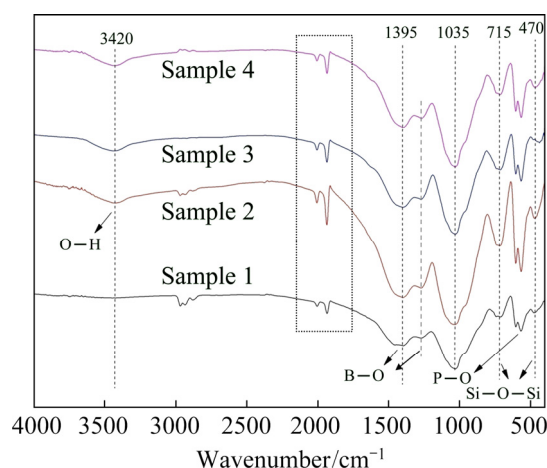


**Fig. 4** FTIR spectra of glass-ceramics with different contents of Rb

Figure 5 shows the SEM images of glass-ceramics with different Rb contents after heat treatment at 720 °C for 6 h. Without addition of Rb, the crystal morphology is rod-like, of which some crystals are bundled or agglomerated together (Figs. 5(a, b)). After addition of 3% Rb, fine grains are formed in the glass matrix, with grain size between 25 and 200 nm (Figs. 5(c, d)) and most of the grain size is under 50 nm. Short-rod-like crystals and regular round particles are formed with size of 70–250 nm with 6% Rb addition (Figs. 5(e, f)). When adding 10% Rb, both rod-like crystals and round particles are observed in the glass-ceramic (Figs. 5(g, h)). The rod-like crystals are longer and the round particles in the glass-ceramic with 10% Rb (270–800 nm in size) are much bigger than those in glass-ceramic with 6% Rb and 3% Rb. As the content of Rb increases, the size of the crystals increases. Mg-whitlockite crystals belong to hexagonal or rhombohedral crystal system [25]. In SEM observation, they show either hexagonal plates [26] or rhombohedral shape [27,28]. Although the XRD results (Fig. 2) show that there is Mg-whitlockite phase in glass-ceramic samples without Rb, there is no obvious Mg-whitlockite crystals observed under SEM. This is probably because the amount of Mg-whitlockite crystals is too little or their sizes are too small to be observed. Since the hydroxyapatite is the only phase in Rb-containing glass-ceramics detected by XRD (Fig. 2), these crystals observed by SEM are all hydroxyapatite crystals. The addition of Rb promotes the nucleation and growth of hydroxyapatite crystals.

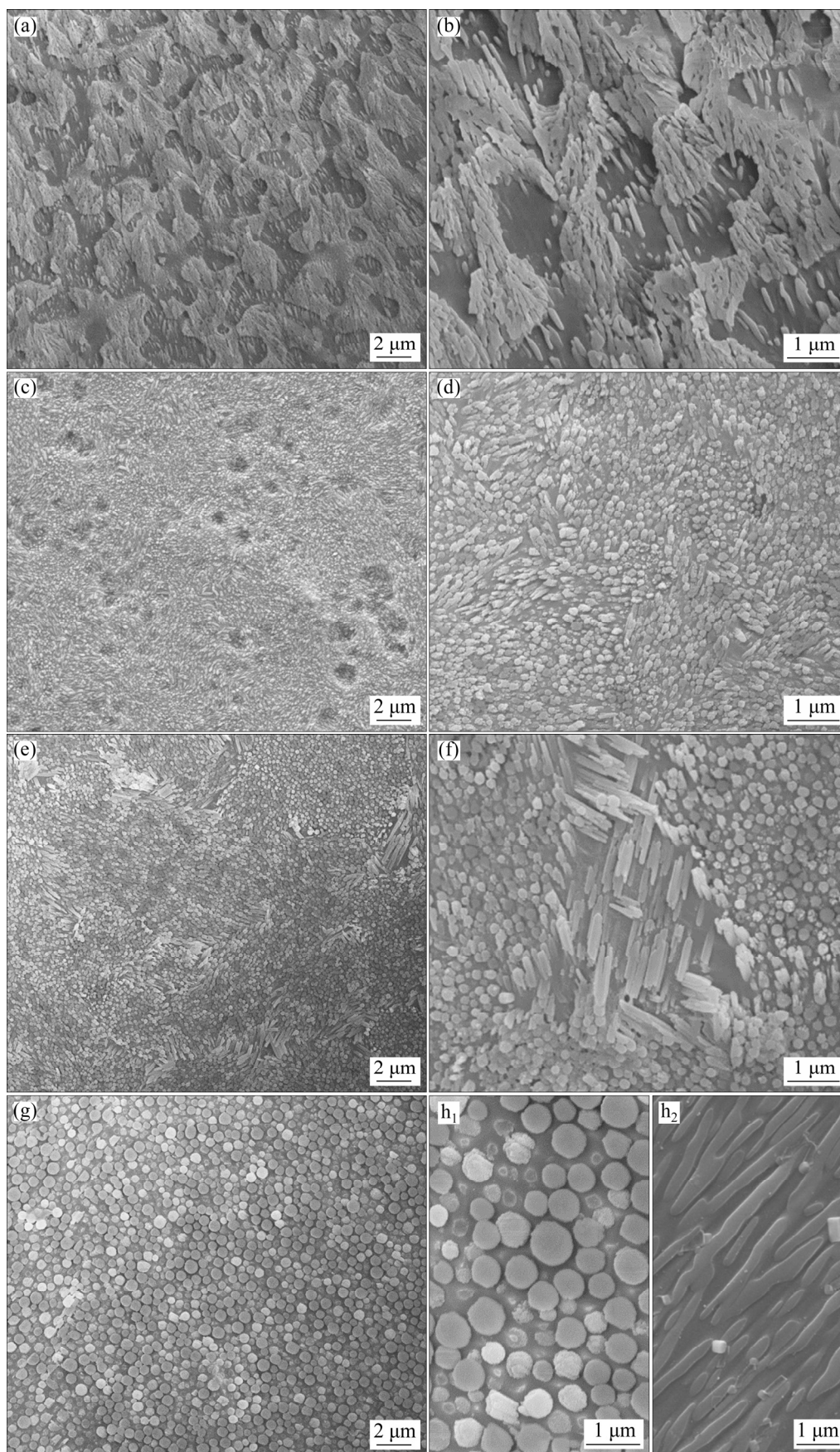


**Fig. 5** SEM images of glass-ceramics with different contents of Rb after heat treatment: (a, b) Sample 1; (c, d) Sample 2; (e, f) Sample 3; (g, h<sub>1</sub>, h<sub>2</sub>) Sample 4

Figure 6 shows the bending strength of the four groups of glass-ceramics. With increasing Rb content, the bending strength increases. The bending strength of all the samples with addition of Rb is higher than that of samples without Rb. The glass-ceramic with 3% Rb exhibits the highest bending strength. According to the Hall–Petch formula, the strength of a material is inversely proportional to the grain size. The grain size of the Rb-containing glass-ceramics increases along with the Rb content (Fig. 5), so the bending strength of the glass-ceramics decreases accordingly.

Figure 7 shows the SEM images of the surface of glass-ceramics soaked in SBF for 7 d. The surface of all the glass-ceramics are completely

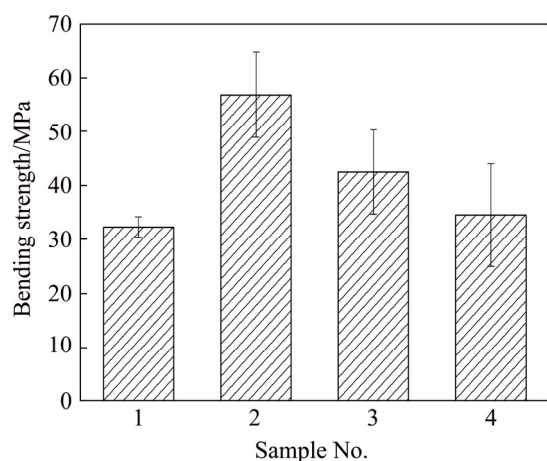
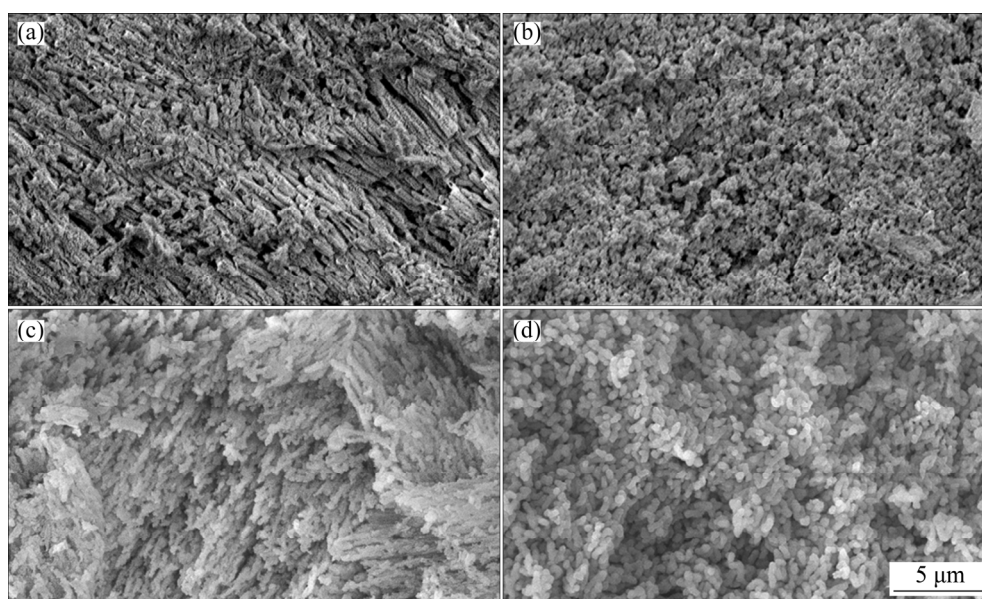


**Fig. 6** Bending strength of glass-ceramics with different contents of Rb

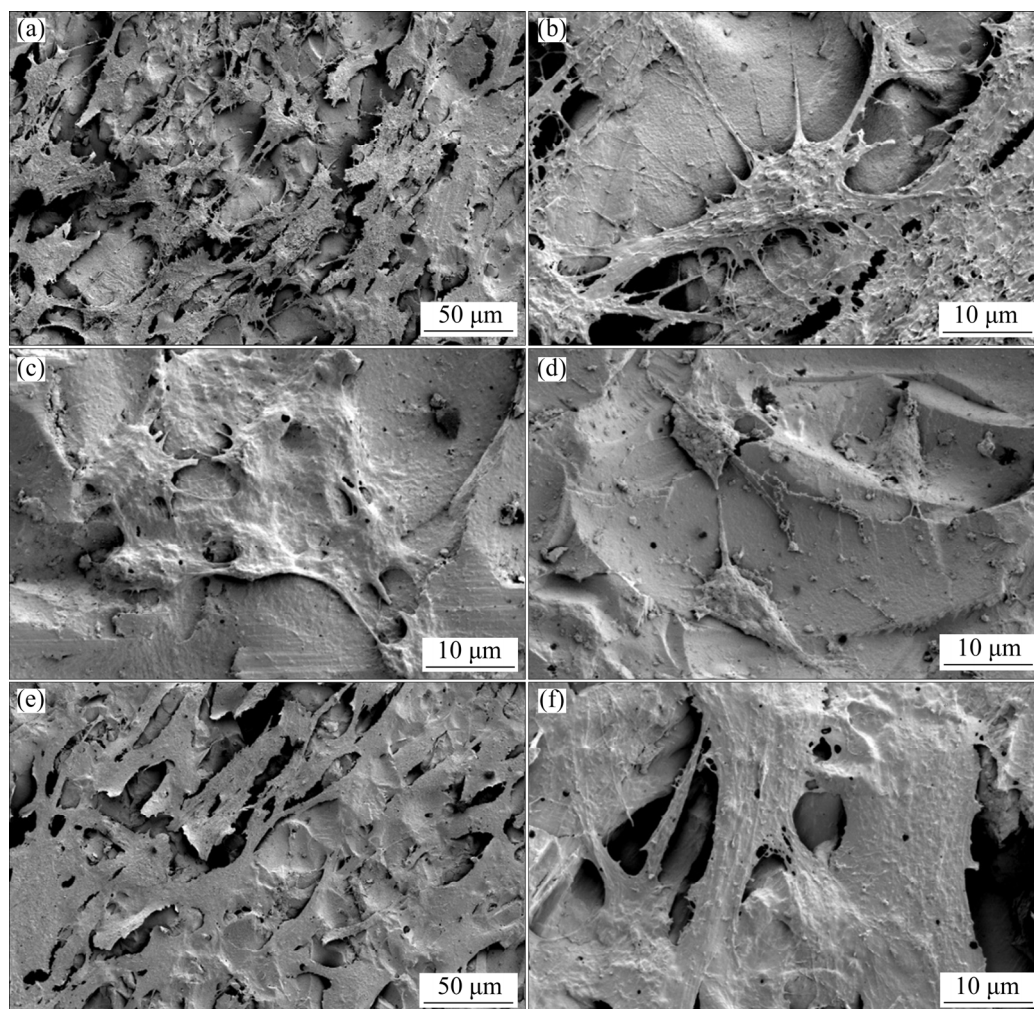
covered by a thick layer of precipitation minerals, with the rough and porous microstructure, including spherical and irregular particles. Since the ceramic crystalline phase in the glass-ceramic is HA, it is a little difficult to characterize the phase of the precipitation layers. But, they can be presumed to be HA. It is assumed that glass-ceramics could form close chemical bond with bone by inducing surface mineralization after implantation.

Figure 8 shows the hBMSCs attachment on the surfaces of glass-ceramics. The cells attach and spread well on the surfaces of all the samples with obvious filopodia extension. This indicates that the glass-ceramics can promote cellular initial adhesion and spreading. The fluorescent results of the staining of cell nuclei and cytoskeleton after 1 d (Figs. 9(a, c, e, g)) and 7 d (Figs. 9(b, d, f, h)) cultivation show that the cell density for all the tested samples increases after 7 d cultivation compared with that after 1 d. However, the cell density for the Rb-containing glass-ceramic (Sample 4) both after 1 and 7 d cultivation is significantly higher than that for the Rb-free glass-ceramic (Sample 1). Especially, after 7 d cultivation, the cells on the surface of Sample 4 reach a confluence. This indicates that Rb addition can promote the cellular proliferation.

The cell viabilities and the ALP activities of hBMSCs after culturing on Samples 1 and 4 for different durations are shown in Fig. 10. In general,



**Fig. 7** SEM images of surfaces of glass-ceramics with different contents of Rb after soaking into SBF for 7 d: (a) Sample 1; (b) Sample 2; (c) Sample 3; (d) Sample 4



**Fig. 8** SEM images of hBMSCs cultured for 24 h on glass-ceramics with different contents of Rb: (a, b) Sample 1; (c) Sample 2; (d) Sample 3; (e, f) Sample 4

both the cell viabilities and the ALP activities increase with prolonging cultivation time. This demonstrates that the samples are not toxic and the cell proliferation is promoted. There is no significant difference in the ALP activities of both groups after 1 and 3 d. However, after 7 d, the ALP activity of the glass-ceramic with Rb (Sample 4) is much higher than that of the Rb-free glass-ceramic (Sample 1). As ALP is regarded as an early marker of osteogenic differentiation, the ALP production can present the osteoblastic differentiation of hBMSCs. Therefore, it is suggested that the addition of Rb can promote the osteoblastic differentiation and the glass-ceramic has osteogenic effect.

The only crystalline phase in Rb-containing glass-ceramics prepared in this work is hydroxyapatite, which is the main inorganic

component of human bone and teeth. Therefore, the samples exhibit excellent biocompatibility, which is confirmed by the cell culture results. It is noteworthy that the samples containing more Rb possess enhanced ability in stimulating cell adhesion and proliferation, as well as osteoblastic differentiation. Some ions have been reported to be beneficial for the interactivity with cells and in vivo bone regeneration. For example, Sr ions can improve osteoblast proliferation and simultaneously reduce osteoclast activity, as well as enhance the bone formation in vivo [29]. It has been reported that lithium (Li) can enhance the proliferation and ALP activity of osteoblasts when adding it to 45S5 glass [30]. The presence of other alkali metals such as sodium and potassium also have been proven to improve the biocompatibility and bioactivity of glass-ceramics [31]. However, the effect of Rb

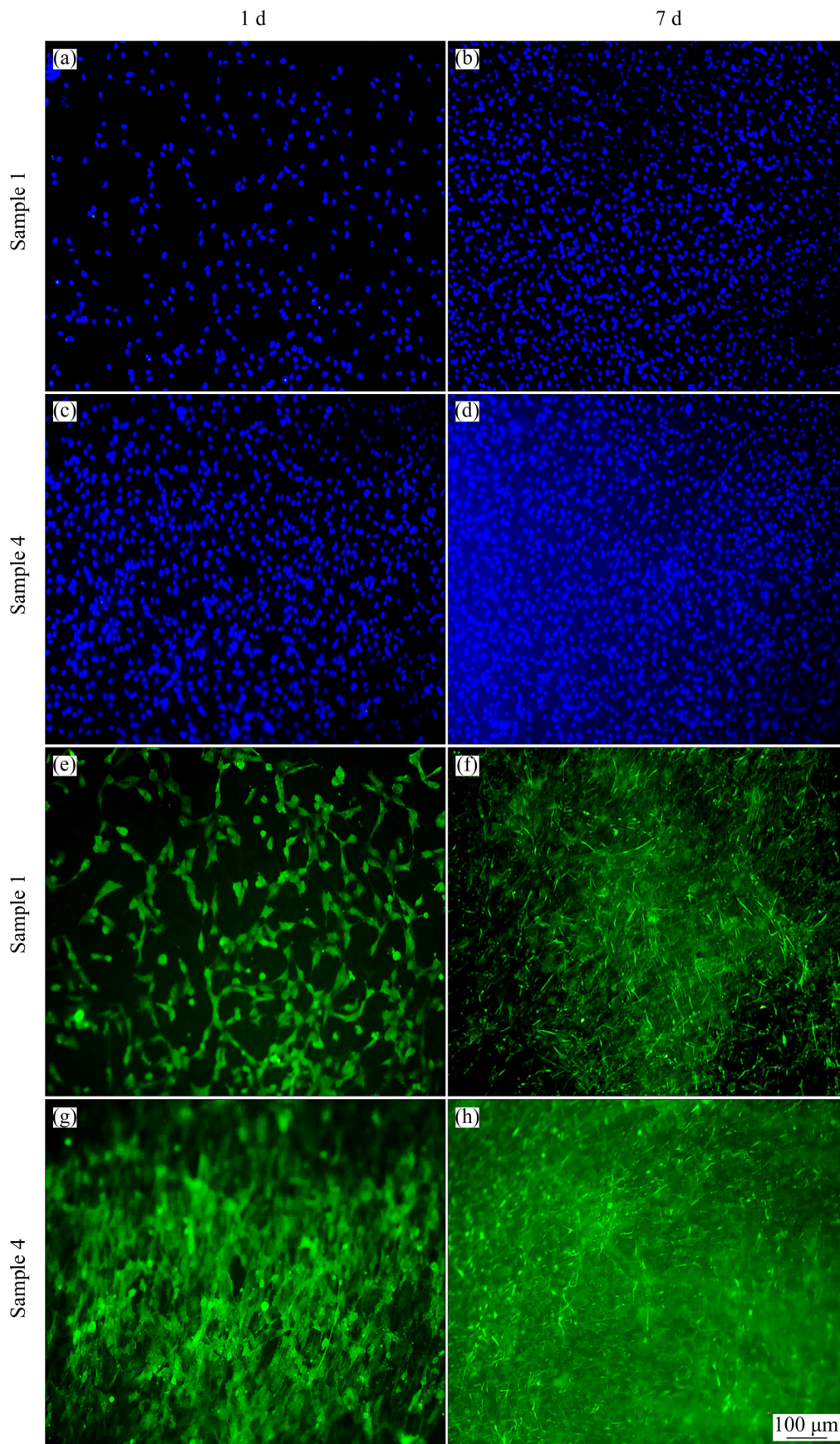


**Fig. 9** Immunofluorescent images of hBMSCs cultured for 1 and 7 d on Samples 1 and 4 with cell nuclei stained by DAPI (a–d, blue) and cytoskeleton stained by FITC-phalloidin (e–h, green)

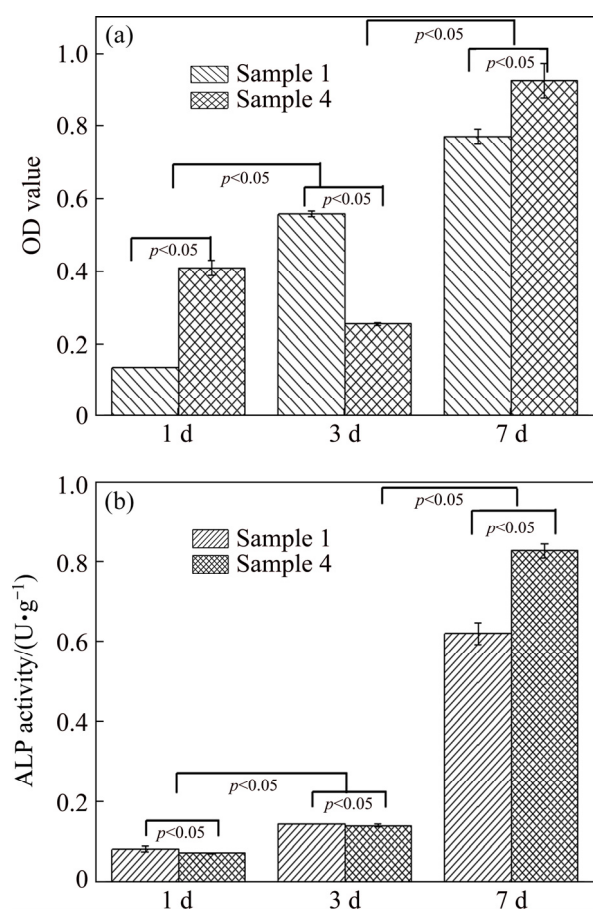


**Fig. 10** Cell viability (a) and ALP activity (b) of hBMSCs cultured on Samples 1 and 4 for 1, 3 and 7 d

addition or doping in biomaterials has been rarely studied. As the main group element same with Li and K, Rb is considered to have the similar biological effect as a doping element or additive. RbCl has been reported to inhibit osteoclastogenesis and promote osteoblastogenesis both in vivo and in vitro by targeting at Jnk/p38-mediated NF- $\kappa$ B activation [32]. In the previous work, Rb has been added into bioglass scaffold [18]. The results show that Rb addition can improve the proliferation and differentiation of hBMSCs by influencing the Wnt/ $\beta$ -catenin signaling pathway. The Rb-containing bioglass has angiogenic and osteogenic effect. In the present work, even though no osteogenic agent was added into the culture medium, the results confirm that Rb addition in glass-ceramics can promote the adhesion, proliferation and ALP activity of hBMSCs on the surface of glass-ceramics. Rb can be employed as a promising doping element for biomaterials to improve their biological performance.

## 4 Conclusions

(1) Glass-ceramics containing different contents of Rb are successfully prepared. Hydroxyapatite crystals are formed in the glass matrix.

(2) The addition of Rb promotes the nucleation and growth of hydroxyapatite crystals. Compared with the glass-ceramics without Rb, Rb-containing glass-ceramics exhibit higher bending strength. Most importantly, Rb addition can promote the cell proliferation and adhesion, and increase the ALP activity.

(3) Rb-containing glass-ceramics with hydroxyapatite crystals can be used in dental or bone repair applications.

## Acknowledgments

The authors are grateful for the financial supports from the Natural Science Foundation of Hunan Province, China (2019JJ50797), and the Postdoctoral Science Foundation of China (2019T120711).

## References

- [1] KAMITAKAHARA M, OHTSUKI C, INADA H, TANIHARA M, MIYAZAKI T. Effect of ZnO addition on bioactive CaO–SiO<sub>2</sub>–P<sub>2</sub>O<sub>5</sub>–CaF<sub>2</sub> glass-ceramics containing apatite and wollastonite [J]. *Acta Biomaterialia*, 2006, 2(4): 467–471.
- [2] HENCH L L, SPLINTER R J, ALLEN W C, GREENLEE T K. Bonding mechanisms at the interface of ceramic prosthetic materials [J]. *Journal of Biomedical Materials Research*, 1971, 5(6): 117–141.
- [3] BASUDEB K. Functional glasses and glass-ceramics: 7–Glasses and glass-ceramics for biomedical applications [M]. Butterworth-Heinemann, 2017: 253–280.
- [4] MUKHOPADHYAY S. Fundamental biomaterials: Ceramics: 6–Bioactive glass-ceramics [M]. Woodhead Publishing, 2018: 129–152.
- [5] RABIEE S M, NAZPARVAR N, AZIZIAN M, VASHAEE D, TAYEBI L. Effect of ion substitution on properties of bioactive glasses: A review [J]. *Ceramics International*, 2015, 41(6): 7241–7251.
- [6] BELLUCCI D, SOLA A, GAZZARRI M, CHIELLINI F, CANNILLO V. A new hydroxyapatite-based biocomposite for bone replacement [J]. *Materials Science and Engineering C*, 2013, 33(3): 1091–1101.
- [7] LU X N, KOLZOW J, CHEN R R, DU J C. Effect of solution condition on hydroxyapatite formation in evaluating bioactivity of B<sub>2</sub>O<sub>3</sub> containing 45S5 bioactive glasses [J]. *Bioactive Materials*, 2019, 4: 207–214.

- [8] NESCAKOVA Z, ZHENG K, LIVERANI L, NAWAZ Q, GALUSKOVA D, KANKOVA H, MICHALEK M, GALUSEK D, BOCCACCINI A R. Multifunctional zinc ion doped sol-gel derived mesoporous bioactive glass nanoparticles for biomedical applications [J]. *Bioactive Materials*, 2019, 4: 312–321.
- [9] KUMARI C V, SOBHANACHALAM P, JAYASANKAR C K, VEERAI AH N, KUMAR V R. Bioactive properties of CuO doped CaF<sub>2</sub>-CaO-B<sub>2</sub>O<sub>3</sub>-P<sub>2</sub>O<sub>5</sub>-MO (M=Ba, Sr, Zn, Mg) glasses [J]. *Ceramics International*, 2017, 43(5): 4335–4343.
- [10] JAGAN MOHINI G, SAHAYA BASKARAN G, RAVI KUMAR V, PIASECKI M, VEERAI AH N. Bioactivity studies on TiO<sub>2</sub>-bearing Na<sub>2</sub>O-CaO-SiO<sub>2</sub>-B<sub>2</sub>O<sub>3</sub> glasses [J]. *Materials Science and Engineering C*, 2015, 57: 240–248.
- [11] BELLANTONE M, WILLIAMS H D, HENCH L L. Broad-spectrum bactericidal activity of Ag<sub>2</sub>O-doped bioactive glass [J]. *Antimicrobial Agents and Chemotherapy*, 2002, 46(6): 1940–1945.
- [12] GENTLEMAN E, FREDHOLM Y C, JELL G, LOTFIBAKHSHAIESH N, O'DONNELL M D, HILL R G, STEVENS M M. The effects of strontium-substituted bioactive glasses on osteoblasts and osteoclasts in vitro [J]. *Biomaterials*, 2010, 31(14): 3949–3956.
- [13] WU C T, ZHOU Y H, LIN C C, CHANG J, XIAO Y. Strontium-containing mesoporous bioactive glass scaffolds with improved osteogenic/cementogenic differentiation of periodontal ligament cells for periodontal tissue engineering [J]. *Acta Biomaterialia*, 2012, 8(10): 3805–3815.
- [14] TAN Yan-ni, LIU Yong. Properties and research progress of rubidium and its compounds [J]. *The Chinese Journal of Nonferrous Metals*, 2017, 27(2): 272–281. (in Chinese)
- [15] SU Y, CHEN L J, HE J Q, YUAN X J, CEN Y L, SU F X, TANG L Y, ZHANG A H, CHEN W Q, LIN Y, WANG S M, REN Z F. Urinary rubidium in breast cancers [J]. *Clinica Chimica Acta*, 2011, 412(23–24): 2305–2309.
- [16] NASTARAN K, ARYA H M, SHAYAN A, SATTAR O, MEHDI K, MOHAMMAD S, AHMAD R D. Elevated level of nitric oxide mediates the anti-depressant effect of rubidium chloride in mice [J]. *European Journal of Pharmacology*, 2015, 762: 411–418.
- [17] CHEN M K, WU S S, TAN Y N, LI R C, LIU Y, HUANG Q L. Rubidium-doped titanium surfaces with modulatory effects on MC3T3-E1 cell response and antibacterial capacity against *Staphylococcus aureus* [J]. *Biomedical Materials*, 2019, 14(4): 1–9.
- [18] HE X, LIU Y, TAN Y N, GROVER L M, SONG J, DUAN S L, ZHAO D P, TAN X F. Rubidium-containing mesoporous bioactive glass scaffolds support angiogenesis, osteogenesis and antibacterial activity [J]. *Materials Science and Engineering C*, 2019, 105: 1–11.
- [19] HE X, DING Y F, XIE W J, SUN R Y, HUNT N C, SONG J, SUN X X, PENG C, ZENG Q H, TAN Y N, LIU Y. Rubidium-containing calcium alginate hydrogel for antibacterial and diabetic skin wound healing applications [J]. *ACS Biomaterials Science & Engineering*, 2019, 5(9): 4726–4738.
- [20] GUO Y, TAN Y N, LIU Y, LIU S F, ZHOU R, TANG H C. Low modulus and bioactive Ti/alpha-TCP/Ti-mesh composite prepared by spark plasma sintering [J]. *Material Science and Engineering C*, 2017, 80: 197–206.
- [21] AGUILAR-REYES E A, LEÓN-PATIÑO C A, VILLICAÑA-MOLINA E, MACÍAS-ANDRÉS V I, LEFEBVRE L P. Processing and in vitro bioactivity of high-strength 45S5 glass-ceramic scaffolds for bone regeneration [J]. *Ceramics International*, 2017, 43(9): 6868–6875.
- [22] AGATHOPOULOS S, TULYAGANOV D U, VENTURA J M, KANNAN S, KARAKASSIDES M A, FERREIRA J M. Formation of hydroxyapatite onto glasses of the CaO-MgO-SiO<sub>2</sub> system with B<sub>2</sub>O<sub>3</sub>, Na<sub>2</sub>O, CaF<sub>2</sub> and P<sub>2</sub>O<sub>5</sub> additives [J]. *Biomaterials*, 2006, 27(9): 1832–1840.
- [23] TERNANE R, COHEN-ADAD M T, PANCZER G, GOUTAUDIER C, KBIR-ARIGUIB N, TRABELSI-AYEDI M, FLORIAN P, MASSIOT D. Introduction of boron in hydroxyapatite: Synthesis and structural characterization [J]. *Journal of Alloys and Compounds*, 2002, 333(1): 62–71.
- [24] WANG Y C, YAO A H, HUANG W H, WANG D P, ZHOU J. In situ fabrication of hollow hydroxyapatite microspheres by phosphate solution immersion [J]. *Journal of Crystal Growth*, 2011, 327(1): 245–250.
- [25] GOPAL R, CALVO C, ITO J, SABINE W K. Crystal structure of synthetic Mg-whitlockite, Ca<sub>18</sub>Mg<sub>2</sub>H<sub>2</sub>(PO<sub>4</sub>)<sub>14</sub> [J]. *Canadian Journal of Chemistry*, 1974, 52(7): 1155–1164.
- [26] GUO X H, LIU X, GAO H C, SHI X T, ZHAO N R, WANG Y J. Hydrothermal growth of whitlockite coating on β-tricalcium phosphate surfaces for enhancing bone repair potential [J]. *Journal of Materials Science & Technology*, 2018, 34(6): 1054–1059.
- [27] KIM H D, JANG H L, AHN H Y, LEE H K, PARK J, LEE E S, LEE E A, JEONG Y H, KIM D G, NAM K T, HWANG N S. Biomimetic whitlockite inorganic nanoparticles-mediated in situ remodeling and rapid bone regeneration [J]. *Biomaterials*, 2017, 112: 31–43.
- [28] JANG H L, JIN K, LEE J, KIM Y, NAHM S H, HONG K S, NAM K T. Revisiting whitlockite, the second most abundant biomineral in bone: Nanocrystal synthesis in physiologically relevant conditions and biocompatibility evaluation [J]. *ACS Nano*, 2014, 8(1): 634–641.
- [29] DENRY I, GOUDOURI O M, FREDERICKS D C, AKKOUCH A, ACEVEDO M R, HOLLOWAY J A. Strontium-releasing fluorapatite glass-ceramic scaffolds: Structural characterization and in vivo performance [J]. *Acta Biomaterialia*, 2018, 75: 463–471.
- [30] KHORAMI M, HESARAKI S, BEHNAMGHADER A, NAZARIAN H, SHAHRABI S. In vitro bioactivity and biocompatibility of lithium substituted 45S5 bioglass [J]. *Materials Science and Engineering C*, 2011, 31: 1584–1592.
- [31] TRANDAFIR D L, PONTA O, CICEO-LUCACEL R, SIMON V. Effects of sodium and potassium ions on a novel SeO<sub>2</sub>-B<sub>2</sub>O<sub>3</sub>-SiO<sub>2</sub>-P<sub>2</sub>O<sub>5</sub>-CaO bioactive system [J]. *Journal of Molecular Structure*, 2015, 1080: 111–116.
- [32] OUYANG Z X, HUANG Q L, LIU B, WU H, LIU T, LIU Y. Rubidium chloride targets Jnk/p38-mediated NF-kappa B activation to attenuate osteoclastogenesis and facilitate osteoblastogenesis [J]. *Frontiers in Pharmacology*, 2019, 10: 1–12.

## 用于骨再生的铷改性生物活性玻璃陶瓷

谭彦妮, 陈文娟, 韦伟, 黄千里, 和祥

中南大学 粉末冶金国家重点实验室, 长沙 410083

**摘要:** 为了研究铷(Rb)元素对  $\text{CaO-SiO}_2\text{-Na}_2\text{O-B}_2\text{O}_3\text{-MgO-ZnO-P}_2\text{O}_5$  系生物玻璃陶瓷的相组成、显微结构、力学性能和细胞响应的影响, 设计加铷和不加铷的玻璃陶瓷成分。结果表明, 在不含 Rb 的生物玻璃陶瓷基体中形成羟基磷灰石(HA)和 Mg-白磷钙矿( $\text{Ca}_{18}\text{Mg}_2\text{H}_2(\text{PO}_4)_{14}$ )晶相; 而添加 Rb 后, 仅检测到 HA 相。添加 Rb 后, 生物玻璃陶瓷中晶体的晶粒尺寸增大。添加 Rb 可以提高生物玻璃陶瓷的抗弯强度。细胞实验结果显示, 含 Rb 的生物玻璃陶瓷具有更好的细胞粘附、增殖和碱性磷酸酶(ALP)活性。总之, 含 Rb 玻璃陶瓷具有良好的力学性能、优良生物活性和生物相容性, 有望应用于骨再生领域。

**关键词:**  $\text{CaO-SiO}_2\text{-Na}_2\text{O-B}_2\text{O}_3\text{-MgO-ZnO-P}_2\text{O}_5$ ; 铷; 生物活性玻璃陶瓷; 羟基磷灰石; 人骨髓间充质干细胞

(Edited by Bing YANG)